

Plasmon dynamics in graphene

Authors: Suheng Xu^{1†*}, Birui Yang^{1†}, Nishchhal Verma¹, Rocco A. Vitalone¹, Brian Vermilyea², Miguel Sánchez Sánchez^{1,3}, Julian Ingham¹, Ran Jing^{4,5}, Yinming Shao^{1,11}, Tobias Stauber³, Angel Rubio^{6,7,8}, Milan Delor⁹, Mengkun Liu^{4,10}, Michael M. Fogler², Cory R. Dean¹, Andrew Millis^{1,7}, Raquel Queiroz¹, D. N. Basov^{1*}

Affiliations:

¹*Department of Physics, Columbia University, New York, New York 10027, USA*

²*Department of Physics, University of California at San Diego, La Jolla, CA 92093-0319, USA*

³*Instituto de Ciencia de Materiales de Madrid ICMM-CSIC, Madrid, Spain*

⁴*Department of Physics and Astronomy, Stony Brook University, Stony Brook, New York 11794, USA*

⁵*Condensed Matter Physics and Materials Science Department, Brookhaven National Laboratory, Upton, New York 11973, USA*

⁶*Theory Department, Max Planck Institute for Structure and Dynamics of Matter and Center of Free-Electron Laser Science, 22761 Hamburg, Germany*

⁷*Center for Computational Quantum Physics, The Flatiron Institute, 162 5th Avenue, New York, New York 10010, USA*

⁸*Nano-Bio Spectroscopy Group, Universidad del País Vasco UPV/EHU, San Sebastián 20018, Spain*

⁹*Department of Chemistry, Columbia University, New York, NY, 10027, USA*

¹⁰*National Synchrotron Light Source II, Brookhaven National Laboratory, Upton, New York 11973, USA*

¹¹*Department of Physics, Pennsylvania State University, University Park, PA, 16802, USA*

†These authors contributed equally to the work

*Corresponding authors: Suheng Xu: sx2277@columbia.edu, D. N. Basov: db3056@columbia.edu

ABSTRACT. Plasmons are collective oscillations of mobile electrons. Using terahertz spacetime metrology, we probe plasmon dynamics of mono- and bi-layer graphene. In both systems, the experimentally measured Drude weight systematically exceeds the prediction based on non-interacting electronic system. This enhancement is most pronounced at ultra-low carrier densities. We attribute the observed deviation to pseudospin dynamics of the Dirac fermions in multi-layer graphene, which leads to a breakdown of Galilean invariance. Our results establish that pseudospin structure of the single-particle electronic wave function can directly govern collective excitations, with implications that extend beyond graphene to a broad class of quantum materials.

I. INTRODUCTION.

In 1900, Paul Drude introduced a classical model of electronic transport that accurately describes conductivity and long-wavelength plasmonic oscillations in metals [1]. This surprising accuracy of Drude model is linked to Galilean invariance, a foundational principle governing transport and collective excitations in solids. Galilean invariance is generally broken in crystals, where the presence of lattices breaks the continuous translational symmetry. However, systems with parabolic electronic bands and trivial quantum geometry typically display an emergent Galilean invariance. The net effect is that single particle descriptions provide an adequate account of the electronic transport which is fundamentally governed by Coulomb interaction [2]. Specifically, in Galilean-invariant systems the plasmon dynamics is solely determined by single particle quantities--- the carrier density and band mass, without corrections from electron-electron interactions [3–12]. In this work we show that

electronic interactions play a fundamental role in collective plasmon dynamics in graphene and link our observations to broken Galilean invariance arising not from energy dispersion but from the structure of the wave functions.

Two-dimensional (2D) materials such as graphene and transition-metal dichalcogenides generally break Galilean invariance because of their non-parabolic dispersions and momentum dependent pseudospin textures [13,14]. Monolayer graphene (MLG) and Bernal bilayer graphene (BLG) are two instructive examples: their single particle electronic states are coherent superpositions of different orbitals across sublattices or layers, with a momentum-dependent phase. For an N -layer graphene system, the conduction-band wavefunction can be written as $|\psi_k\rangle = (|a_k\rangle + |b_k\rangle e^{Ni\phi_k})/\sqrt{2}$, where ϕ_k is the azimuthal angle of in-plane momentum (k_x, k_y) . [13,15]. Here, $|a_k\rangle$ and $|b_k\rangle$ represent orbitals localized onto the two sublattices in MLG, or the two layers in BLG. As shown in Fig.1(b,d), the pseudospin $n_k = (\cos(N\phi_k), \sin(N\phi_k), 0)$ winds

once and twice around the Brillouin zone for MLG and BLG, respectively. This momentum-space vortex structure transforms non-trivially under a change of reference frame (Fig. 1(h-j)), signaling broken Galilean invariance. The nontrivial transformation properties reflect the underlying quantum geometry and are responsible for the theoretically predicted renormalization of plasmon dispersion in Ref. [6]. The impacts of graphene's nontrivial electronic structure on collective electron dynamics is anticipated to be strongest in the vicinity of charge neutrality point. Indeed, at charge neutrality, orbital mixing and the attendant quantum geometrical properties of the wavefunction are most evident. Thus, the experimental studies of the plasmon renormalization carried out in very weakly doped graphene provide a direct pathway for exploring quantum geometric effects in the collective responses.

Here, we use nascent technique of nano-THz spacetime metrology [16,17] to investigate plasmon dynamics in MLG and BLG. By visualizing the spacetime trajectories (worldlines) of plasmonic waves, we extract plasmon velocities and the Drude weight as a function of the carrier density. We find that both MLG and BLG exhibit a density-dependent enhancement of the Drude weight relative to noninteracting theory predictions. Contrary to conventional expectations that interactions suppress charge motion, the observed enhancement reveals a non-trivial interplay between electron-electron correlations and quantum geometry. These findings establish plasmonic worldline metrology as a powerful tool for probing many-body correlations in solids in space and time.

II. METHODS

We employ scattering-type scanning near-field optical microscope (s-SNOM) [18] to visualize propagating plasmons at THz frequencies far below the diffraction limit [supplemental materials]. This technique accesses large in-plane momenta with a spatial resolution of \sim 20-50nm [19]. As illustrated in Fig. 1e, picosecond THz pulses spanning the range between 0.5-1.5 THz illuminate both the sample and the metalized atomic force microscope (AFM) tip [20-25]. Raster-scanning the sample beneath the tip yields two-dimensional maps of the local THz response of hBN-encapsulated BLG (Fig. 1f). The scattered THz amplitude from BLG exceeds that of the SiO_2 substrate, confirming its the high conductivity under back-gate modulation.

In our experiments, plasmons are launched by tip-sample near-field coupling. These propagating plasmonic wave packets travel radially from the tip,

reflect at the graphene edge, and return to the tip. To capture this motion, we utilize nano-THz spacetime mapping [16,17]. This latter technique provides a direct measurement of plasmon velocity, which reflects the Drude weight of the electron liquid in graphene as we will discuss below. Fig. 1g shows a representative plasmonic spacetime map acquired for BLG at $V_{bg} - V_{CNP} = 15V$, $T=38K$. Line cuts at fixed time delays (solid lines in Fig 1g) reveal the propagating wave packets. The false-color scale encodes the measured electric field strength of the plasmon wave packet, proportional to the local charge density variation. The horizontal axis corresponds to the tip position along the white dashed line in Fig. 1f, with the shaded region marking the SiO_2 substrate beyond the BLG edge. The slope of the worldlines quantifies the plasmon group velocity v_g , while the temporal decay of the field amplitude along the worldline determines the plasmon lifetime [supplemental material].

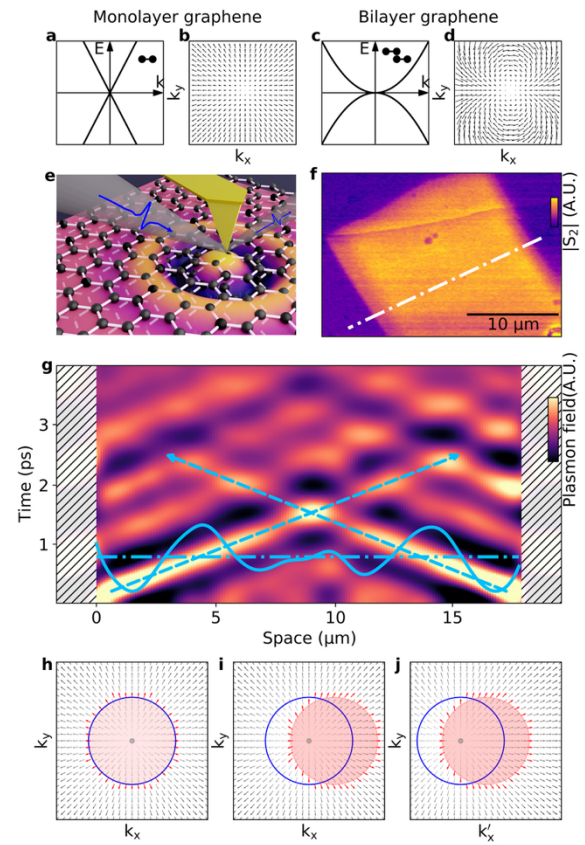


Figure 1 Spacetime dynamics of plasmons, pseudospin textures in graphene and broken Galilean invariance. (a) The single-particle electronic band structure of MLG. (b) Pseudospin of MLG in momentum space. (c) The single-particle electronic band structure of BLG within a two-band model. (d) Pseudospin of BLG in momentum space. (e) Schematics of THz near-field measurement on a hBN-encapsulated graphene residing on SiO_2/Si substrate. (f) THz near-field image of the BLG sample. The false-color map corresponds to the amplitude of the tip-scattered THz pulses. (g) A

spacetime map of plasmon in BLG measured at $V_{bg} - V_{CNP} = 15V$, $T=38K$. The shaded regions correspond to the substrate area and the false color map shows the plasmon field strength. Panels h-j: Schematics of pseudospin direction for MLG in momentum space, and the occupation states at different space or time in plasmon oscillation. The blue circle depicts the static Fermi surface whereas the red circle is shifted Fermi surface under the influence of the Thz field.

III. RESULTS

We mapped the plasmonic worldlines at $T=45$ K across a range of back-gate voltages. Representative data sets for MLG and BLG at selected V_{bg} are shown in Fig. 2. With increasing V_{bg} , the worldline slopes dt/dx decrease, indicating higher plasmon group velocities. The persistence of plasmon worldlines at CNP is noteworthy. This latter finding enables direct probing of the collective response of the electron liquid in the ultra-dilute regime.

Figures 2b-c display the gate-voltage dependent group velocity extracted from the spacetime measurements. In both systems, v_g decreases toward a minimum value at CNP. At comparable carrier densities, plasmons in MLG propagate faster than those in BLG, reflecting the steeper slope of the electronic Dirac dispersion in MLG. In BLG, the plasmon dispersion further exhibits a pronounced electron-hole asymmetry: plasmons on the electron-doped side (positive V_{bg}) propagate faster than those on the hole-doped side at the same carrier density. This asymmetry arises partly from the intrinsic distinctions between conduction and valance bands in the BLG [26]. In additional, the single back-gate architecture of our devices introduces a finite displacement field at nonzero gate voltage, which is enhanced under hole doping due to intrinsic offset doping but is negligible on the electron side [supplemental material].

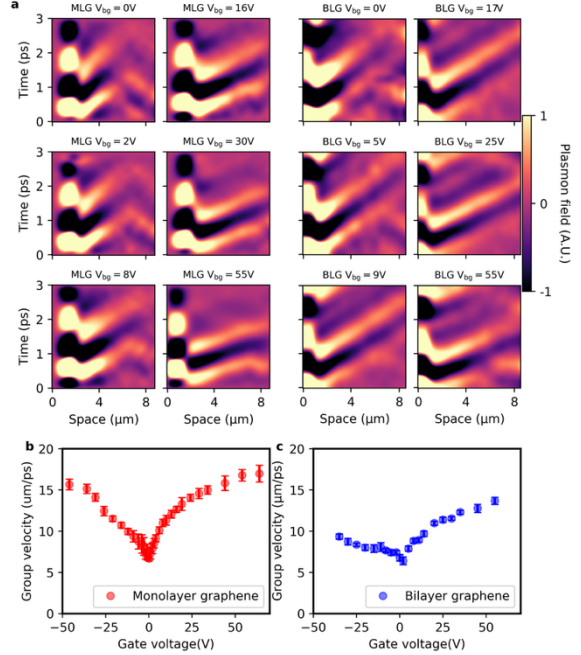


Figure. 2. Gate dependent plasmonic spacetime maps for monolayer and bilayer graphene. (a) Representative spacetime maps for MLG and BLG at selected gate voltages. The spacetime maps are collected at 45K. (b-c) Carrier density dependent group velocity of plasmon in MLG and BLG.

To quantify the electrodynamic response, we evaluate the Drude weight, or the charge stiffness, which characterizes the rigidity of the electron liquid to an applied electric field. The Drude weight is directly extracted from the worldline metrology as $D = \frac{v_g^2 \pi e \epsilon_0}{d}$. (Supplemental material). Here, d is the distance between the graphene layer and the metallic back gate, and ϵ is the dielectric constant of the spacer separating them. In a Galilean invariant system, the Drude weight is given by $D_0 = \frac{e^2 n}{m_0}$, where n is the carrier density and m_0 is the effective mass. Thus, one expects a linear dependence of D on n with a zero intercept as n goes to zero.

Figure 3a-b displays the experimentally extracted Drude weights (D) as a function of the carrier density. We focus on the hole-doped regime due to weaker displacement field effect and more vivid plasmonic features. At doping below $1 - 2 \times 10^{11} cm^{-2}$, as indicated by the shaded region, charge dynamics are dominated by disorder and thermal fluctuations, making an exact determination of the carrier density inaccessible (Supplemental material). For both MLG and BLG, the Drude weight D decreases with decreasing carrier density, but deviates from the linear Galilean-invariant prediction $D_0 = \frac{e^2 n}{m_0}$. This deviation could arise from two factors: (i) the non-

parabolicity of the single-particle band structure, yielding a density-dependent properties, and (ii) many-body corrections rooted in the intertwined charge and pseudospin dynamics. To disentangle these two contributions, we compare our data with the results of the non-interacting theory. In Fig. 3a, the dashed line shows the theoretical Drude weight for MLG with linear Dirac dispersion: $D_0 = \frac{e^2 v_F}{\sqrt{\pi \hbar^2}} \sqrt{n}$, obtained using the bare Fermi velocity $v_F = 0.85 \times 10^6 \text{ m/s}$ [27]. The experimental data systematically exceed the non-interacting prediction, signaling an enhanced effective Fermi velocity of approximately $v_F = 1.15 \times 10^6 \text{ m/s}$ (dot-dashed line).

Fig. 3b presents the Drude weight analysis for BLG, obtained using a four-band tight-binding model with best-fit hopping parameters [28]. The experimentally extracted Drude weights (D) exceed these non-interacting predictions (D_0). We remark that even neglecting interactions, the BLG bands deviate from a simple parabolic form. At low carrier density ($n < 0.4 \times 10^{12} \text{ cm}^{-2}$), trigonal warping splits the double Dirac vortex into a central Dirac vortex accompanied by three satellite vortices [15].

The Drude weight renormalization, quantified by the ratio D/D_0 , is enhanced with decreasing carrier density, as shown in Fig. 3(c-d). In MLG, the enhancement is a weakly density-dependent logarithmic correction (gray dashed line); in BLG the enhanced spectral weight scales approximately as $1/\sqrt{n}$. The Drude weight renormalization, which signals a breakdown of the conventional theory, will be discussed in detail in the next section.

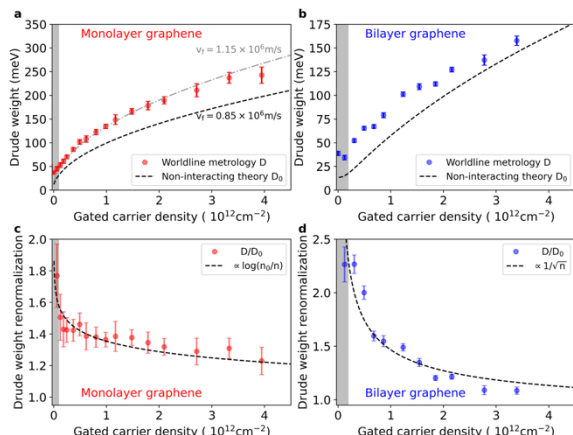


Figure 3. Plasmonic probe of the Drude weight renormalization. (a) Carrier density dependent Drude weight for monolayer graphene. The gray shaded area indicates the disorder-dominated regime. (b) Carrier density dependent Drude weight in bilayer graphene. The gray shaded area indicates the thermal regime. The theoretical estimation assumes the electronic temperature $T=40 \text{ K}$ (c-d) The ratio between the experimentally measured Drude weight and non-

interacting Drude weight in monolayer and bilayer graphene. The dashed traces indicate a phenomenological fit to the carrier density dependent renormalization.

IV. The physics of the Drude weight renormalization

We now show that the Drude weight renormalization in graphene revealed by plasmon dynamics (Figs. 2,3) can be understood as a consequence of the pseudospin physics. A plasmon corresponds to oscillations of current and charge. At equilibrium, the Fermi surface is centered at $k = 0$, with a radius set by carrier density (blue circles in Figs. 1h). An electric current corresponds to the momentum-space shift of the Fermi surface (red circle in Figs. 1h,i). In conventional 2D electron gases, Galilean invariance ensures that such a shift leaves the internal structure of the wave function unchanged, so plasmon dynamics is governed by the center-of-mass motion and scales as n/m_0 .

By contrast, in both MLG and BLG, shifting the Fermi surface alters the pseudospin over the entire Fermi surface (Fig. 1i). A simple coordinate transformation (Fig. 1j) cannot restore the original configuration, revealing the breakdown of Galilean invariance. Consequently, plasmonic oscillations are inherently coupled to sublattice (MLG) or interlayer (BLG) degrees of freedom. The energy cost associated with these pseudospin rearrangements stiffens the plasmon mode, thereby increasing its propagation velocity [6]. Thus, our THz metrology data establish a direct link between the plasmonic response and the pseudospin texture of the electron wavefunction in the presence of electron-electron interactions.

The coupling between charge and pseudospin dynamics modifies the current response, a process that can be understood within perturbation theory [6]. We schematically show these corrections in Fig. 4a. Drude weight is given by the static, long-wavelength limit of the current-current correlator, quantifying the ability of an applied electric field to generate particle-hole excitations. In the non-interacting limit, it is captured by an intra-band response and depends entirely by the single-particle band dispersion (middle panel in Fig. 4a). Interactions, however, open additional pathways for the creation of particle-hole excitations.

In the first order in perturbation theory, interactions may lead to two distinct types of corrections. The self-energy corrections (left panel in Fig. 4a) dress the electronic Greens function, renormalizing the quasiparticle dispersion effectively reshaping the band structure. The vertex corrections (right panel in Fig. 4a)

modify the coupling between electrons and external photons. The latter process --- also referred to as Drude-interband mixing [5,29] --- represents the generation of intraband current via virtual interband transitions mediated by Coulomb interaction. Unlike self-energy corrections, the vertex corrections are not captured by probes such as Shubnikov-de Haas oscillations or angle-resolved photoemission spectroscopy [3]. Yet, we find that the inter-/intraband mixing manifests in THz space-time metrology (Figs.2,3).

In Galilean-invariant system, self-energy and vertex corrections cancel exactly, leaving the Drude weight immune to electron-electron interactions to all orders in perturbation theory [3–12]. In MLG and BLG, however, Galilean invariance is broken by the momentum-dependent pseudospin structure, and this precarious cancellation of interaction effects no longer occurs. As a result, Drude weight acquires a genuine new geometric contribution due to the coupling between charge and pseudospin dynamics through the Coulomb interaction.

To further quantify the Drude weight renormalization in MLG and BLG, we explicitly compute the first-order corrections[supplemental material]. Fig. 4b shows the calculated Drude weight renormalization in MLG for different dielectric constant ϵ , representing different Coulomb interaction strength, modeled as $v_q = e^2/2\epsilon\epsilon_0 q$. In the limit of complete screening ($\epsilon \rightarrow \infty$), the renormalization vanishes. At finite ϵ , however, the Drude weight is enhanced, with the effect becoming stronger at lower carrier densities or smaller screening constants. The enhancement follows a logarithmic dependence on carrier density, consistent with experimental data. Using an effective screening constant $\epsilon = \frac{\epsilon_{top} + \epsilon_{sub}}{2} = \frac{1+5}{2} = 3$, the theory predicts an averaged renormalization factor of 1.3-1.4 at carrier density $n = 1 - 2 \times 10^{12} \text{ cm}^{-2}$. Including intrinsic screening in graphene would slightly increase the effective ϵ to ~ 6 , bringing the theory into better quantitative agreement with our measurements.

Fig. 4c presents the corresponding calculation for BLG, modeled within a two-band approximation with realistic hopping parameters. Unlike MLG, BLG has a finite density of states at the CNP, so electron-electron interactions are relatively short-ranged. In this case, the Thomas-Fermi screening remains finite even at charge neutrality, giving a Coulomb interaction of the form $v_q = e^2/2\epsilon\epsilon_0(q + \eta q_{TF})$, where η is a phenomenological parameter interpolating between

the full static Thomas-Fermi limit ($\eta = 1$) and weaker screening. In the $\eta = 1$ case, the Coulomb interaction is short-ranged, and the Drude-weight renormalization is suppressed. By contrast, our experiments show enhancements of 25-50% at carrier density $1 - 2 \times 10^{12} \text{ cm}^{-2}$, indicating a weaker effective screening. Finally, we note that the precise magnitude of Drude-weight renormalization in BLG might depend sensitively on the non-parabolic details of its band structure and on realistic screening conditions. A complete quantitative theory that incorporates these effects remains an open problem for future work.

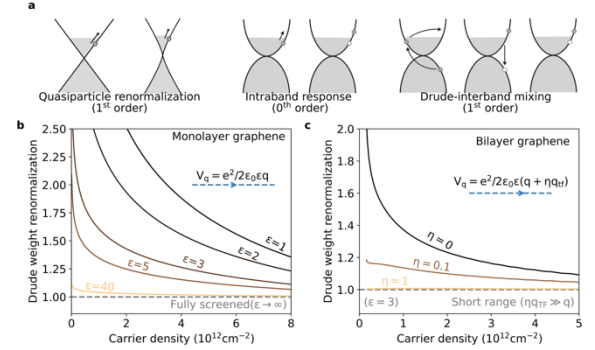


Figure 4. Diagrammatic interpretation of Drude weight renormalization. (a) Diagrammatic interpretation of many-body pathways for Drude weight enhancement. (b) Calculated Drude weight renormalization in monolayer. The false color scale on multiple curves represents long-range Coulomb interaction with varying dielectric constants ϵ . (c) Calculated Drude weight renormalization in bilayer. The false color scale on the curve corresponds to a Thomas-Fermi approximation for different screening strength. A substrate screening constant $\epsilon = 3$ is used in the calculation.

Finally, we remark that the observed enhancement of Drude weight is a non-trivial phenomenon. Conventional many-body theory usually predicts that interaction suppress electronic motion, reducing the mobility, as commonly observed in ordinary solids. A notable recent counterexample is the enhancement of superfluid density in flat-band systems, which is attributed to the combined effects of interactions and nontrivial quantum geometry [30]. The Drude weight enhancement reported here represents a complementary manifestation. Extending space-time metrology to probing collective mode dynamics in other platforms, such as twisted bilayer graphene or moiré transition-metal dichalcogenides, remains an important direction for future investigations.

ACKNOWLEDGMENTS

Funding:

Research on THz electrodynamics of graphene at Columbia is supported as part of Programmable Quantum Materials, an Energy Frontier Research

Center funded by the U.S. Department of Energy (DOE), Office of Science, Basic Energy Sciences (BES), under award DE-SC0019443. Development of THz instrumentation at Columbia is supported by DOE-BES DE-SC0018426. Fabrication of plasmonic structures, is supported by W911NF2510062 (R.V., D.N.B.).

Author contributions:

S.X. and D.N.B. conceived the study. S.X. recorded the near-field data with support from R.A.V. . B.Y. prepared the graphene sample with guidance from C.D.. N.V. performed theoretical calculation with assistance from B.V., M.S.S., J.I., T.S., A.R., M.M.F, A.J.M, R.Q.. S.X. analyzed the data with assistance

from N.V.,R.A.V,R.J.,Y.S.,M.D.,M.L.. S.X. and D.N.B. wrote the manuscript with input from all coauthors.

Competing interests:

The authors declare that they have no competing interests.

Data and materials availability:

All data needed to evaluate the conclusions in the paper are present in the paper and/or the Supplementary materials.

Reference

- [1] P. Drude, Zur Elektronentheorie der Metalle, Ann. Phys. **306**, 566 (1900).
- [2] M. GREITER, F. WILCZEK, and E. WITTEN, HYDRODYNAMIC RELATIONS IN SUPERCONDUCTIVITY, Mod. Phys. Lett. B **3**, 903 (1989).
- [3] T. Okabe, Electrical Conductivity of Fermi Liquids. I. Many-Body Effect on the Drude Weight, J. Phys. Soc. Jpn. **67**, 2792 (1998).
- [4] A. Yurtsever, V. Moldoveanu, and B. Tanatar, Dynamic correlation effects on the plasmon dispersion in a two-dimensional electron gas, Phys. Rev. B **67**, 115308 (2003).
- [5] W.-K. Tse and A. H. MacDonald, Interaction effects in the optical conductivity of bilayer graphene: Drude-interband coupling and screening, Phys. Rev. B **80**, 195418 (2009).
- [6] S. H. Abedinpour, G. Vignale, A. Principi, M. Polini, W.-K. Tse, and A. H. MacDonald, Drude weight, plasmon dispersion, and ac conductivity in doped graphene sheets, Phys. Rev. B **84**, 045429 (2011).
- [7] P.-M. Zhang and P. A. Horvathy, Kohn's theorem and Galilean symmetry, Phys. Lett. B **702**, 177 (2011).
- [8] L. S. Levitov, A. V. Shtyk, and M. V. Feigelman, Electron-electron interactions and plasmon dispersion in graphene, Phys. Rev. B **88**, 235403 (2013).
- [9] T. Stauber, P. Parida, M. Trushin, M. V. Ulybyshev, D. L. Boyd, and J. Schliemann, Interacting Electrons in Graphene: Fermi Velocity Renormalization and Optical Response, Phys. Rev. Lett. **118**, 266801 (2017).
- [10] T. Stauber, G. Gómez-Santos, and L. Brey, Plasmonics in Topological Insulators: Spin-Charge Separation, the Influence of the Inversion Layer, and Phonon-Plasmon Coupling, ACS Photonics **4**, 2978 (2017).
- [11] X. Li and W.-K. Tse, Theory of interaction-induced renormalization of Drude weight and plasmon frequency in chiral multilayer graphene, Phys. Rev. B **95**, 085428 (2017).
- [12] A. Mu, Z. Sun, and A. J. Millis, Optical conductivity of the two-dimensional Hubbard model: Vertex corrections, emergent Galilean invariance, and the accuracy of the single-site dynamical mean field approximation, Phys. Rev. B **106**, 085142 (2022).
- [13] C.-H. Park and N. Marzari, Berry phase and pseudospin winding number in bilayer graphene, Phys. Rev. B **84**, 205440 (2011).
- [14] H. Min, G. Borghi, M. Polini, and A. H. MacDonald, Pseudospin magnetism in graphene, Phys. Rev. B **77**, 041407 (2007).

[15] E. McCann and M. Koshino, The electronic properties of bilayer graphene, *Rep. Prog. Phys.* **76**, 056503 (2013).

[16] S. Xu et al., Electronic interactions in Dirac fluids visualized by nano-terahertz spacetime interference of electron-photon quasiparticles, *Sci. Adv.* **10**, (2024).

[17] S. Anglhuber et al., Spacetime Imaging of Group and Phase Velocities of Terahertz Surface Plasmon Polaritons in Graphene, *Nano Lett.* **25**, 2125 (2025).

[18] R. Hillenbrand, Y. Abate, M. Liu, X. Chen, and D. N. Basov, Visible-to-THz near-field nanoscopy, *Nat. Rev. Mater.* **1** (2025).

[19] X. Chen, D. Hu, R. Mescall, G. You, D. N. Basov, Q. Dai, and M. Liu, Modern Scattering-Type Scanning Near-Field Optical Microscopy for Advanced Material Research, *Adv Mater* **325**, 1804774 (2019).

[20] H. T. Stinson et al., Imaging the nanoscale phase separation in vanadium dioxide thin films at terahertz frequencies, *Nat Commun* **9**, 1 (2018).

[21] T. L. Cocker, V. Jelic, R. Hillenbrand, and F. A. Hegmann, Nanoscale terahertz scanning probe microscopy, *Nat Photonics* **15**, 558 (2021).

[22] J. Zhang et al., Terahertz Nanoimaging of Graphene, *Acs Photonics* **5**, 2645 (2018).

[23] R. Jing et al., Terahertz response of monolayer and few-layer WTe₂ at the nanoscale, *Nat Commun* **12**, 5594 (2021).

[24] M. Eisele, T. L. Cocker, M. A. Huber, M. Plankl, L. Viti, D. Ercolani, L. Sorba, M. S. Vitiello, and R. Huber, Ultrafast multi-terahertz nano-spectroscopy with sub-cycle temporal resolution, *Nat Photonics* **8**, 841 (2014).

[25] R. A. Vitalone et al., Charge Transfer Plasmonics in Bespoke Graphene/α-RuCl₃ Cavities, *ACS Nano* **25**, 29648 (2024).

[26] J. Li, L. Z. Tan, K. Zou, A. A. Stabile, D. J. Seiwell, K. Watanabe, T. Taniguchi, S. G. Louie, and J. Zhu, Effective mass in bilayer graphene at low carrier densities: The role of potential disorder and electron-electron interaction, *Phys. Rev. B* **94**, 161406 (2016).

[27] D. N. Basov, M. M. Fogler, A. Lanzara, F. Wang, and Y. Zhang, Colloquium: Graphene spectroscopy, *Rev Mod Phys* **86**, 959 (2014).

[28] J. Jung and A. H. MacDonald, Accurate tight-binding models for the π bands of bilayer graphene, *Phys. Rev. B* **89**, 035405 (2014).

[29] B. V. Bondarev, *Density Matrix Theories in Quantum Physics* (2020).

[30] P. Törmä, S. Peotta, and B. A. Bernevig, Superconductivity, superfluidity and quantum geometry in twisted multilayer systems, *Nat. Rev. Phys.* **4**, 528 (2022).